AIAA JOURNAL
Vol. 32, No. 11, November 1994

Flow Structure in the Wake of a Wishbone Vortex Generator

B. J. Wendt* and W. R. Hingst†
NASA Lewis Research Center, Cleveland, Ohio 44135

The results of an experimental examination of the vortex structures shed from a low-profile "wishbone" generator are presented. The vortex generator height relative to the turbulent boundary layer was varied by testing two differently sized models. Measurements of the mean three-dimensional velocity field were conducted in cross-stream planes downstream of the vortex generators. In all cases a counter-rotating vortex pair was observed. Individual vortices were characterized by three descriptors derived from the velocity data: circulation, peak vorticity, and cross-stream location of peak vorticity. Measurements in the cross plane at two axial locations behind the smaller wishbone characterize the downstream development of the vortex pairs. A single region of streamwise velocity deficit is shared by both vortex cores. This is in contrast to conventional generators, where each core coincides with a region of velocity deficit. The measured cross-stream velocities for each case are compared with an Oseen model with matching descriptors. The best comparison occurs with the data from the larger wishbone.

Background and Research Objectives

VORTEX generators are used to provide a measure of flow control. Most often the goal is to achieve some resistance to boundary-layer separation or to reduce the deleterious effects of locally strong secondary flows.

In external flow situations, such as that encountered on airfoils, the most common application is upstream of flight control surfaces where boundary-layer attachment is often critical to flight performance.

In internal flows, vortex generators are used to prevent flow separation and to reduce total pressure distortion. These effects occur often in inlet ducts and diffusers, due to such factors as duct centerline curvature and large changes in duct cross-sectional area.

The key to vortex generator performance is in the mixing and secondary velocity field created downstream by the shed vortex structures. If properly situated in the flowfield, the helical motion of the fluid in the vortex forces high-energy fluid of the freestream into the slower moving fluid of the boundary layer while countering the tendency of naturally occurring secondary flows to distort the flowfield by the opposite mechanism, namely, to displace boundary-layer fluid away from the wall and into core regions of the flow.

Since the vortex generator presents an obstruction in the flow, there is a drag penalty paid for its use. Conventional blade type or delta wing type vortex generators are found to work best when the vortex generator height above the flow surface h is approximately that of the local boundary-layer thickness δ. Recent work in the design and performance of vortex generators has produced low-profile vortex generators that meet or exceed the mixing and strength performance of more conventional types. The height ratio h/δ for a low-profile vortex generator is typically between one-tenth and three-tenths, thereby providing a substantial reduction in the drag penalty paid for its use.[1] Low-profile vortex generators have been used recently to control a shock/boundary-layer interaction[2] and to improve the total pressure distortion and recovery performance of a diffusing S-duct.[3] Figure 1 illustrates the use of a "wishbone" generator, which is a particularly effective low-profile design. The secondary velocity structure of the shed vortices is measured in a cross plane downstream of the vortex generator. As indicated in Fig. 1, this structure is a pair of counter-rotating vortices with the flow between vortices directed away from the wall (an "upflow" pair). This structure was verified in a flow visualization study conducted by Lin et al.[4]

Following the work of Westphal et al.,[5] our qualitative description of embedded vortex structure can be quantified using three parameters or "descriptors." For any embedded vortex i these are as follows:

1) (z_i, y_i)—location of the vortex core center. Its variation with axial position x represents the trajectory of the vortex.

2) $\omega_i^{\max}$—peak vorticity. The peak vorticity is located at (z_i, y_i), and its magnitude is indicative of the vortex concentration.

3) Γ_i—circulation of the vortex. Γ_i represents the "spinning strength" of the vortex.

Each of these three descriptors is derivable from the secondary velocity data taken in a downstream cross plane, as illustrated in Fig. 1. A recent study conducted at NASA Lewis Research Center[6] focused on the quantitative description of the vortices shed from conventional vortex generator blades. In this study we conduct a similar examination of the low-profile wishbone generator. The objectives of this study are summarized as follows:

1) Mount a large low-profile wishbone generator in the thick boundary layer of NASA Lewis Research Center's Icing Research Tunnel (IRT). At a suitable position downstream of the vortex generator conduct highly resolved cross-plane velocity surveys to characterize and quantify the vortex structures produced by the generator. Conduct these measurements on two different models,

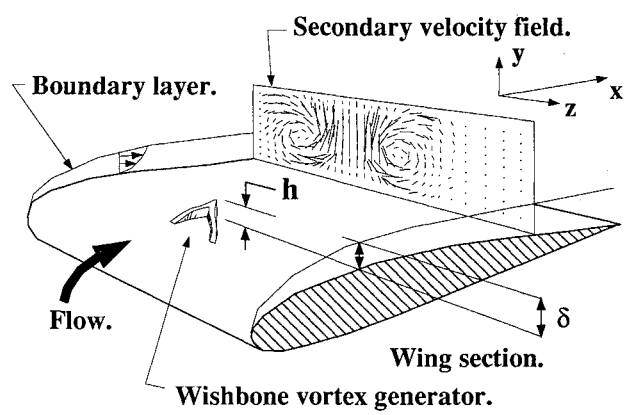

Fig. 1 Flow structures shed from a vortex generator are examined in a downstream cross plane.

Presented as Paper 94-0620 at the AIAA 32nd Aerospace Sciences Meeting, Reno, NV, Jan. 10–13, 1994; received Jan. 31, 1994; revision received May 23, 1994; accepted for publication May 23, 1994.

*National Research Council Associate, Inlet, Duct, and Nozzle Flow Physics Branch, Mail Stop 5-11, 21000 Brookpark Road. Member AIAA.

†Research Engineer, Inlet, Duct, and Nozzle Flow Physics Branch, Mail Stop 5-11, 21000 Brookpark Road. Member AIAA.

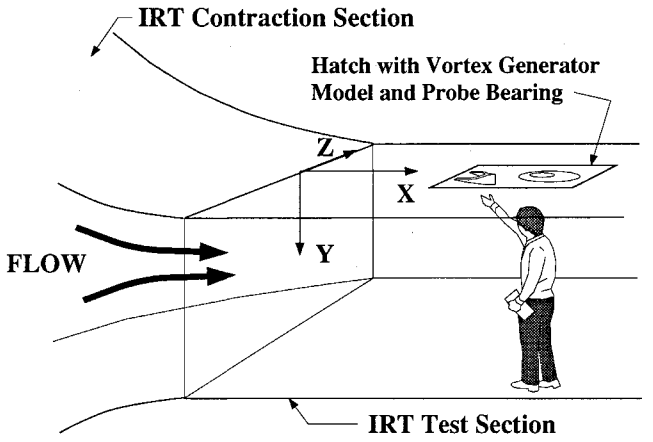

Fig. 2 IRT test section showing the coordinate system used and the location of the test hardware.

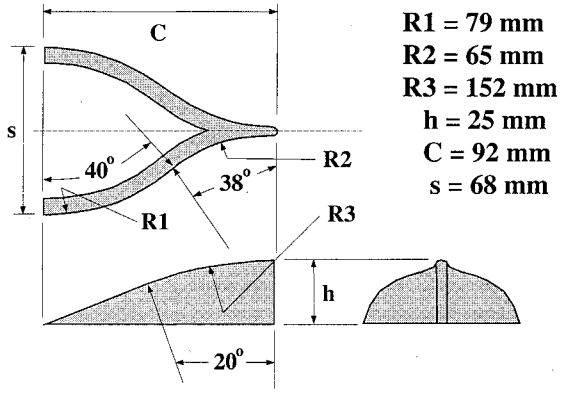

Fig. 3 Small wishbone generator geometry. The dimensions of the larger generator are 2.5 times the values listed here.

varying h/δ. For one model, examine two downstream cross planes to study the streamwise development of these structures.

2) These measurements have the additional benefit of providing workers in computational fluid dynamics a basis for modeling low-profile wishbone generators in their studies. Simple mathematical models, developed in terms of the vortex descriptors, are derived from the data to represent the measured vortex structures as velocity and vorticity distributions. These models are then compared against the data.

Test Parameters and Research Instrumentation

This study was conducted in the NASA Lewis Icing Research Tunnel. Figure 2 is an illustration of the test section showing the coordinate system in use. The Cartesian coordinate axes are centered on the tunnel top wall at an axial location corresponding to the boundary between the contraction and test section. The model vortex generator, probe, and probe traversing hardware are mounted on a hatch in the test section ceiling. The leading edge of this hatch is located at $x \approx 3$ m. This test was conducted at a freestream Mach number of 0.2. The test section freestream velocity U_∞ is approximately 70 m/s.

Boundary-layer surveys conducted in the empty test section indicate a nominally two-dimensional turbulent profile over the central two-thirds span of the top wall. At the axial location corresponding to the mounting position of the vortex generator model $\delta \approx 9$ cm, and the Reynolds number is $Re = U_\infty x/\nu \approx 13 \times 10^6$. The boundary-layer displacement thickness δ^* had a spanwise averaged value of 1.4 cm at this axial location. A variation in δ^* of 4% occurred over the center span region of the test section ceiling.

The vortex generator models tested in this study are patterned after the Wheeler wishbone design.[7] Figure 3 is an illustration of the geometry. Two models were constructed from a block of aluminum alloy using a wire-cutting electric discharge machining process. The dimensions of both models are given in Fig. 3.

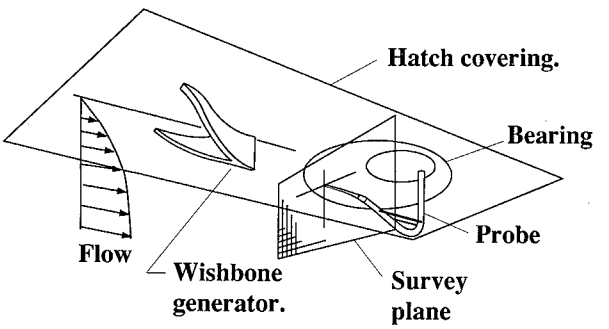

Fig. 4 Arrangement of model generator and instrumentation on the test section ceiling.

Figure 4 illustrates the arrangement of hatch, vortex generator model, velocity probe, and traversing bearing. A two axis (z, y) mechanism located above the hatch moves the probe stem in the cross-plane survey grid, sealed by the free-floating "double-bearing" rig.

The velocity probe is a five-hole pitot probe with a tip diameter of 0.23 cm. This probe tip is mounted off axis on a goose-necked stem to a position upstream of the circular bearing seal line. The probe is used in a non-nulling capacity and is calibrated to determine all three components of the mean flow velocity. Uncertainty in the measured velocities were assessed following the procedure outlined by Reichert and Wendt.[8]

Right and left side flow symmetry in the cross plane is expected in the wake of the vortex generator. To take advantage of this, the survey grids examined in this study are not centered with respect to the model but are positioned to favor the right half. The large vortex generator model is mounted with its trailing edge at (x, z) = (3.24, 0.00) m. The 15.1 × 13.5 cm (z, y) cross-plane survey grid used for the larger model is centered at (x, z) = (3.47, 0.04) m. This is one chord length downstream of the model.

The smaller vortex generator is mounted at two x locations. The (x, z) trailing-edge positions are at (3.10, 0.00) m and (3.38, 0.00) m. The axial variation of δ between these two x positions is negligible. The 11.4 × 10.8 cm grid used for the smaller model is centered at (x, z) = (3.47, 0.04) m for survey locations of four chord lengths and one chord length downstream of the model, respectively. The grid spacing for both models is $\Delta z = \Delta y = 0.64$ cm.

Experimental Results

Small Vortex Generator

The cross-plane velocity field measured one chord length downstream of the small vortex generator ($h/\delta = 0.30$) is shown in Fig. 5a. A concentrated pair of upflow vortices is evident in the vector plot.

The three structural descriptors of the right-hand-side (RHS) vortex are derived from the measured cross-plane velocity field illustrated in Fig. 5a. The velocity field is first converted to a streamwise vorticity field following the relation

$$\omega_x = \left(\frac{\delta w}{\delta y} - \frac{\delta v}{\delta z} \right) \tag{1}$$

where w is the z component of the velocity vector and v the y component. Fourth-order finite difference formulas (second-order on the grid boundary) are used to represent the spatial derivatives in Eq. (1). Figure 5b is the vorticity plot corresponding to the velocity field depicted in Fig. 5a; $\omega_i^{\max}$ is located at a grid point having coordinates (z_i, y_i). For the RHS vortex illustrated in Figs. 5a and 5b,

$$\omega_i^{\max} = 7586 \pm 100 \text{ s}^{-1} \text{ m}$$
$$(z_i, y_i) = 1.44, 2.56 \pm 0.01 \text{ cm} \tag{2}$$

Uncertainty estimates for all descriptors derived from the data are determined by combining the uncertainties in measured velocities

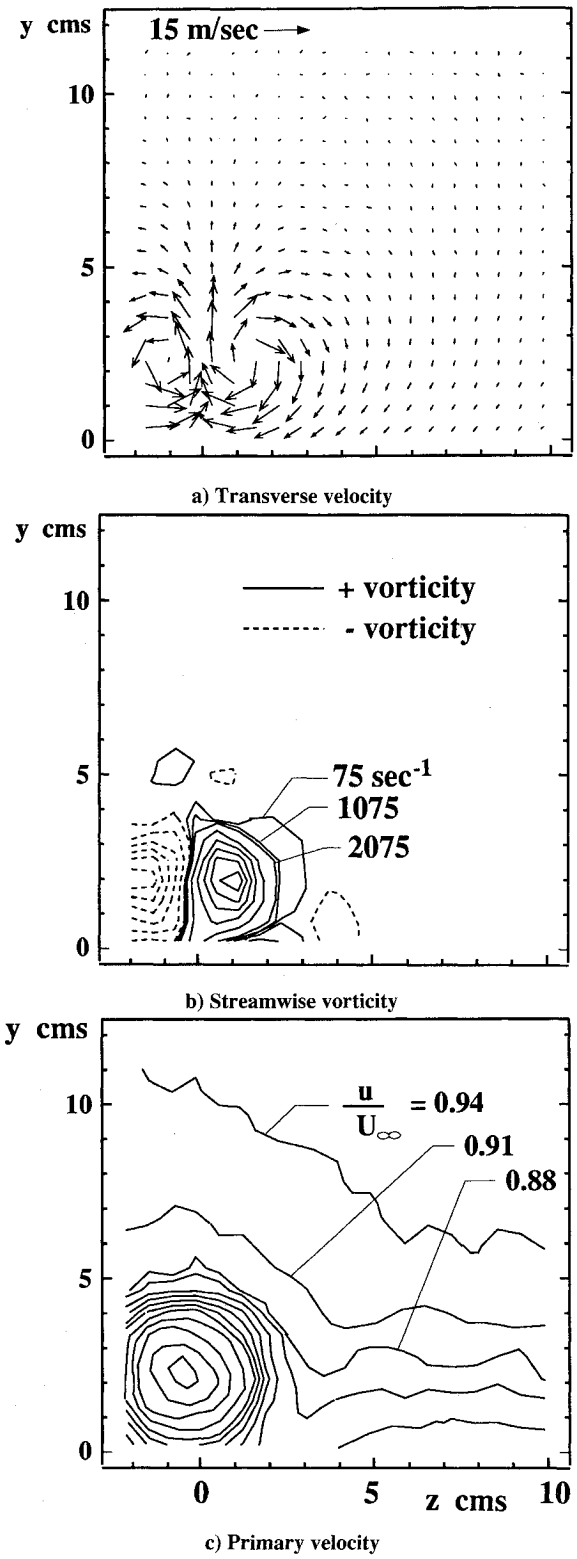

Fig. 5 Results one chord length downstream of the small vortex generator.

and probe positions in accordance with the procedure outlined by Moffat.[9] The center of the vortex appears to be located on the right shoulder of the vortex generator. The circulation Γ_i is calculated by first isolating the region of core vorticity in the data field. This is done by referring to the contour plot in Fig. 5b. A path enclosing the region of core vorticity is defined. The outer boundary of the core is taken to be the location where streamwise vorticity is 1% of the peak core value.The circulation is then calculated according to

$$\Gamma_i = \oint_{\text{path}} V \cdot ds \tag{3}$$

where V is the velocity vector in the cross plane, and s refers to the path coordinate. By using closed paths composed of line segments in the z or y coordinate directions, the circulation is easily determined. The circulation of the vortex illustrated in Fig. 5b is found to be $\Gamma_i = 1.56 \pm 0.05$ m^2/s. Contours of streamwise velocity ratio are plotted in Fig. 5c. The boundary layer is slightly thickened in the vicinity of the embedded upflow pair, as would be expected. An unexpected result is the lack of a streamwise velocity deficit coinciding with the location of each vortex center. A single large region of streamwise velocity deficit encloses both vortex cores and is centered at a cross-plane location coincident with the tip location of the vortex generator.

The corresponding results recorded four chord lengths downstream of the small vortex generator are shown in Figs. 6a–6c. The descriptors of the RHS vortex at this location are

$$\omega_i^{\max} = 1044 \pm 100 \text{ s}^{-1}$$

$$(z_i, y_i) = 2.08, 5.12 \pm 0.01 \text{ cm} \tag{4}$$

$$\Gamma_i = 1.05 \pm 0.05 \text{ m}^2/\text{s}$$

Figures 6a and 6c illustrate the displacement of the vortex cores away from the wall, convected there by the strong secondary flows occurring in the upwash region of the vortex pair. As discussed in Wendt et al.[10] the 33% reduction in circulation may be attributed, in part, to the cross-plane component of wall shear stress that applies a torque opposing the rotation of the vortex. An additional mechanism for the observed circulation decay is the diffusion of vorticity between the closely spaced vortex cores. A steep gradient in streamwise vorticity between the left-hand-side (LHS) and RHS cores is evident in Figs. 5b and 6b. In addition to reducing circulation and peak vorticity, diffusion of the core vorticity has significantly increased the core size as can be seen by comparing Figs. 5 and 6. Located under the core in Fig. 6b is a region of "secondary" vorticity. This vorticity, opposite in sign to that of the core or "primary" vorticity, is induced by the viscous interaction between the secondary flows of the vortex and the wall. Figure 6c again shows a single region of streamwise velocity deficit. This region is now centered between, and above, the vortex cores.

Large Vortex Generator

The results obtained one chord length downstream of the large vortex generator ($h/\delta = 0.70$) are illustrated in Figs. 7a–7c. The descriptors of the RHS vortex are

$$\omega_i^{\max} = 6345 \pm 100 \text{ s}^{-1}$$

$$(z_i, y_i) = 2.74, 8.15 \pm 0.01 \text{ cm} \tag{5}$$

$$\Gamma_i = 5.17 \pm 0.25 \text{ m}^2/\text{s}$$

Modeling

The large number of parameters to consider when designing a vortex generator array for an aircraft component, such as a wing or inlet, has the implication that experimental work on optimum designs is often slow and expensive. This fact has motivated a few workers in computational fluid mechanics to assist in the optimizing problem by including a means of representing vortex generators in their codes. A simple and effective means of doing this is to employ a model for the cross-plane velocity or vorticity induced by the generators. This is the approach taken in recent work by Anderson and Gibb,[11] who examined multiple vortex generator array geometries in a diffusing S-duct inlet using a parabolized Navier-Stokes (PNS) solver. A similar inclusion of embedded vortices in a full Navier-Stokes (FNS) code was implemented by Cho and Greber[12] for a constant area circular duct and a diffusing S-duct geometry. The advantage of this approach lies in the fact that a newly formed vortex may be accurately represented in this manner.

Experimental workers concerned with embedded vortices have often noticed the close similarity of observed cross-plane vortex

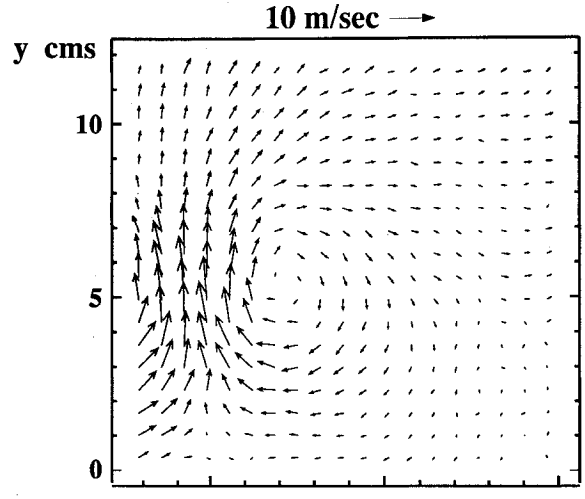

a) Transverse velocity

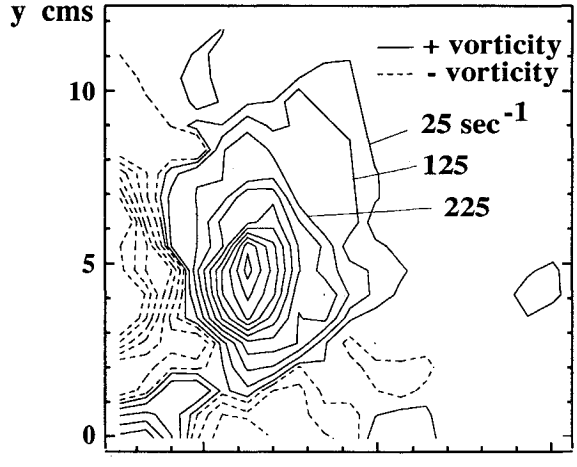

b) Streamwise vorticity

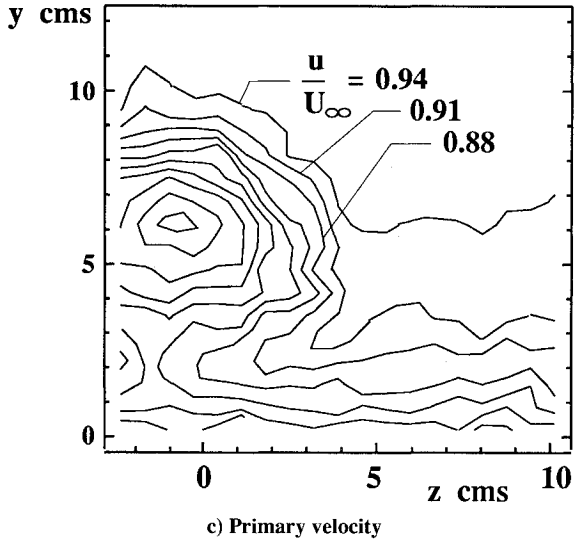

c) Primary velocity

Fig. 6 Results obtained four chord lengths downstream of the small vortex generator.

structure to simple two-dimensional models of vortices. Inviscid or "potential" models were first applied to results obtained in subsonic diffusers by Taylor and Grose.[13] Later, Pearcy[14] would develop embedded vortex interaction models based on the inviscid representation of embedded vortex structure. Eibeck and Eaton[15] compared the structure of a single embedded vortex with that of the patchwork "Rankine" model vortex. Studies by Pauley and Eaton[16] and Wendt et al.[17] have made comparisons to the "ideal viscous" or "Oseen" model.

Let us now examine the equations of the Oseen model and show the comparison between the model and the present results.

Oseen Model of the Embedded Vortex

The two-dimensional Oseen model of a viscous vortex represents the time-dependent decay of a potential vortex where the velocity at the origin ($r = 0$) is forced to zero at time $t = 0$. A single isolated vortex centered on the cross-plane origin has velocity components (in cylindrical coordinates):

$$v_r = 0$$
$$v_\theta = \frac{\Gamma}{2\pi r}[1 - e^{r^2/(4\nu t)}] \text{ m} \tag{6}$$

where Γ is the vortex circulation and ν the laminar coefficient of kinematic viscosity. Following Squire[18] the unsteady solution is transformed to a steady one by relating the decay time to the distance between the vortex generator tip and the cross plane of interest $(x - x_0)$:

$$t \approx \frac{x - x_0}{U_\infty} \tag{7}$$

For an isolated turbulent vortex i located at (z_i, y_i) the velocity components in the cross plane can be written in terms of the vortex descriptors.[17] In Cartesian coordinates,

$$v_i = \frac{\Gamma_i (z - z_i)}{2\pi R_i^2} F_i$$
$$w_i = -\frac{\Gamma_i (y - y_i)}{2\pi R_i^2} F_i \tag{8}$$

where

$$R_i^2 = (z - z_i)^2 + (y - y_i)^2 \tag{9}$$

and

$$F_i = 1 - \exp\left(-\frac{\pi \omega_i^{\max}}{\Gamma_i} R_i^2\right) \tag{10}$$

The vorticity field is given by

$$\omega_i^x = \omega_i^{\max}(1 - F_i) \tag{11}$$

We can superimpose solutions for a representation of the wall and neighboring vortices. Figure 8 illustrates how a representation of a single embedded vortex is constructed. Equations (8) represent the secondary velocities v_i and w_i for the vortex above the wall. The equations for the image vortex are identical except for the sign switch on Γ_i, $\omega_i^{\max}$, and y_i. Denote these velocities $v_{\text{im}i}$ and $w_{\text{im}i}$. The equations representing the embedded vortex are then simply

$$v = v_1 + v_{\text{im}1}$$
$$w = w_1 + w_{\text{im}1} \tag{12}$$

Figure 9 illustrates the construction of an embedded array of N vortices. The secondary velocities of this flowfield are

$$v = v_1 + v_{\text{im}1} + v_2 + v_{\text{im}2} + \ldots + v_N + v_{\text{im}N}$$
$$w = w_1 + w_{\text{im}1} + w_2 + w_{\text{im}2} + \ldots + w_N + w_{\text{im}N} \tag{13}$$

Model and Data Comparisons

The model is constructed by matching the vortex descriptors in the equations to those previously listed for the data [Eqs. (2),

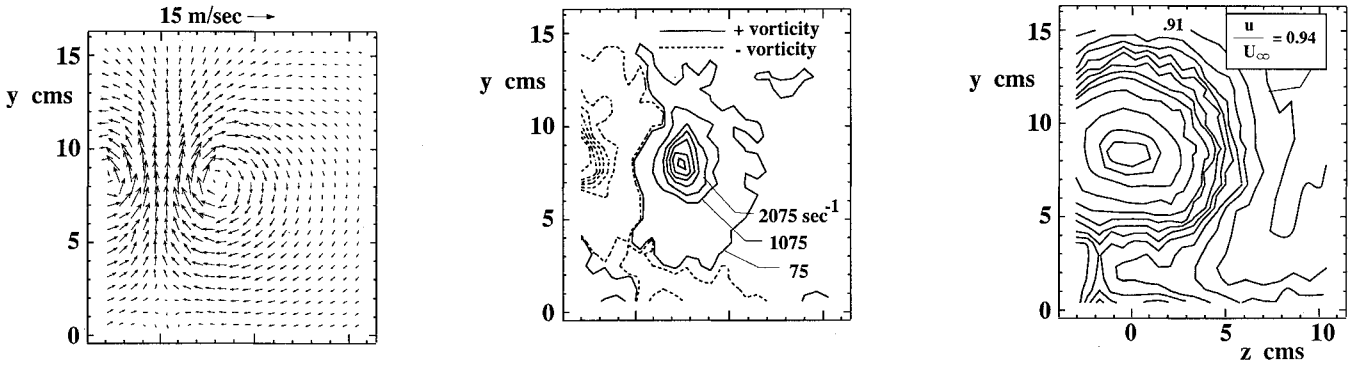

a) Transverse velocity b) Streamwise vorticity c) Primary velocity

Fig. 7 Results obtained one chord length downstream of the large vortex generator.

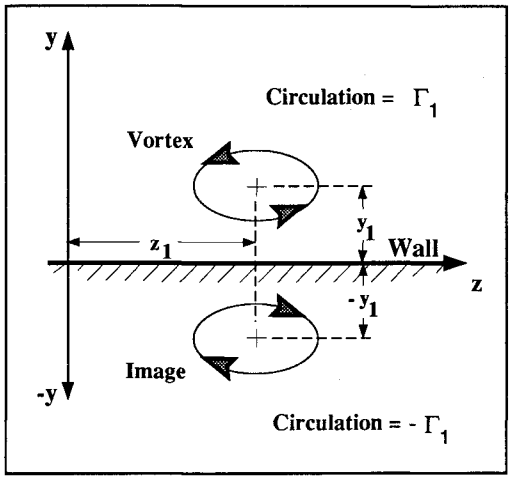

Fig. 8 Construction of an Oseen model of a single embedded vortex.

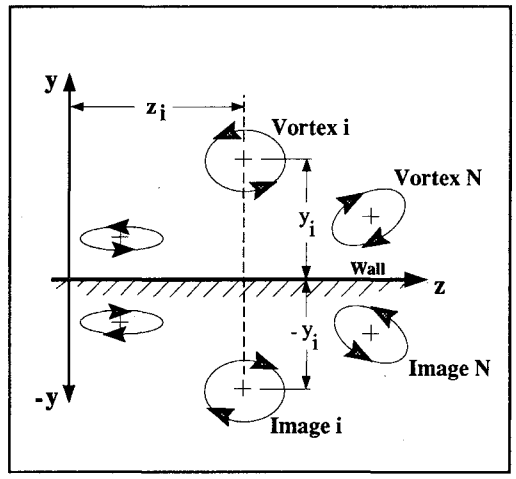

Fig. 9 Construction of an Oseen model of an array of *N* embedded vortices.

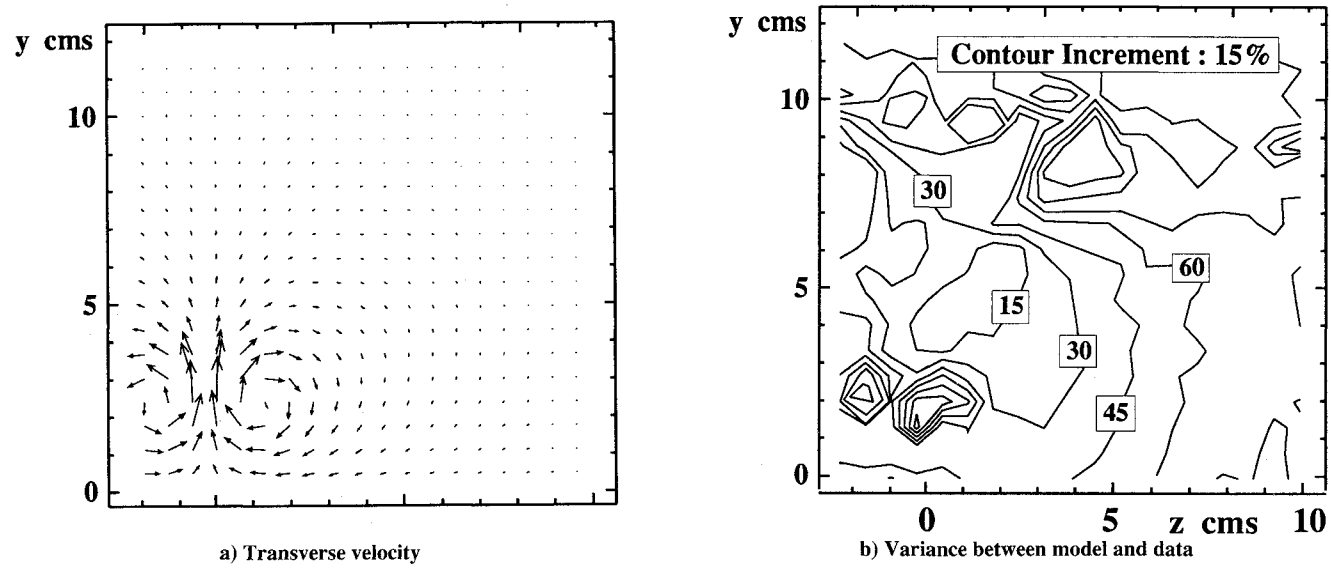

a) Transverse velocity b) Variance between model and data

Fig. 10 Model results one chord length downstream of the small vortex generator.

(4), and (5)].The circulation and peak vorticity descriptors for the LHS vortex in each case are chosen to be equal (but opposite in sign) to the descriptor values determined for the RHS vortex; (z_i, y_i) for the LHS vortex is found by symmetry with respect to the plane $(x, y, z = 0)$.

Figure 10a illustrates the cross-plane velocity field of the model when the vortex descriptors are matched to those obtained from the data taken one chord length downstream of the small vortex generator. This can be compared with Fig. 5a. One point to note is that the near-wall velocities are a good deal weaker in the model representation of the data. Figure 10b is a contour plot of the variance between the data and the model defined as

$$\text{variance} = \frac{\|V_{\text{data}} - V_{\text{model}}\|}{\|V_{\text{data}}\|} \tag{14}$$

The best comparison occurs just above the RHS core, where the variance is less than 15%.

Figures 11a and 11b illustrate the corresponding results for the cross-plane field four chord lengths downstream of the small vor-

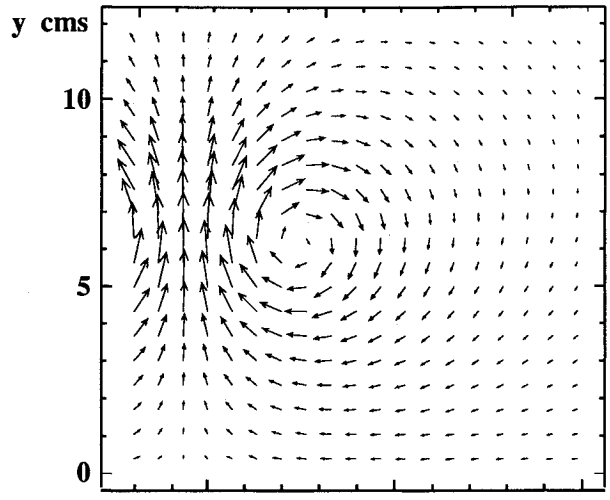

a) Transverse velocity

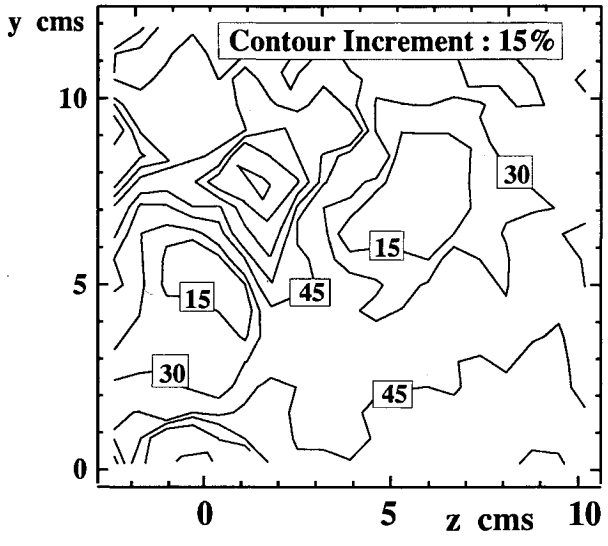

b) Variance between model and data

Fig. 11 Model results four chord lengths downstream of the small vortex generator.

tex generator. Figure 11a may be compared with Fig. 6a. The best comparison here occurs just below the vortex core and to either side.

Figures 12a and 12b illustrate the model and variance obtained one chord length downstream of the large vortex generator. Figure 12a may be compared with Fig. 7a. The model provides a better match to the data in this case, as evidenced by the large regions of the flowfield (in the vortex upwash, downwash, and above the core) where the variance is less than 15%.

The discrepancy between the data and the model originates, in part, with the manner in which the model is constructed. In particular, the equations of the model, Eqs. (6–11), contain no terms to represent the convective effects of crossflow on the vortex cores. This explains the more elongated or elliptical shape of the vortex cores observed in the data plots. In addition to the shape distortion, the model vortices are weaker than their data counterparts. Again, this discrepancy is based on the manner in which the model is constructed, but here the explanation is more subtle. Recall that the model is constructed with an image vortex to represent the influence of the wall. An Oseen vortex possesses a viscous core. When used as an image vortex, a portion of the vorticity field will cancel an equal portion of the vorticity field of the modeled vortex above the wall, thereby reducing the overall strength or circulation of the modeled vortex. This effect becomes more pronounced the closer the vortex core is to the wall or another neighboring vortex. Let us quantify this difference by integrating the vorticity field for these test cases. The modeled vorticity field is, in each test case,

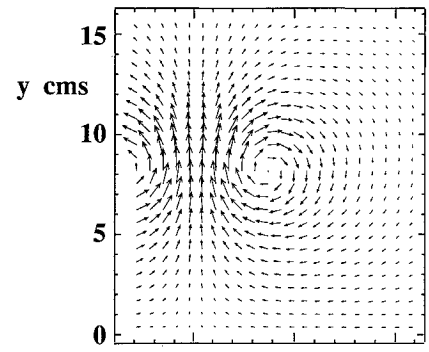

a) Transverse velocity

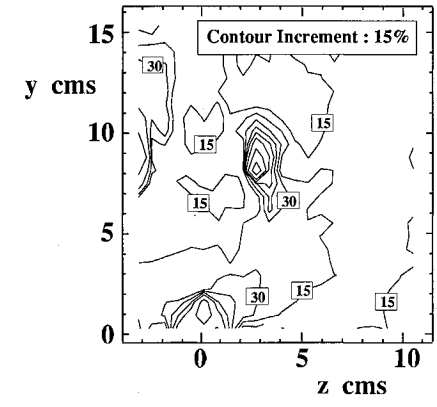

b) Variance between model and data

Fig. 12 Model results one chord length downstream of the large vortex generator.

$$\omega_x = \sum_{i=1}^{2} (\omega_i + \omega_{\mathrm{im}\,i}) \tag{15}$$

To determine the circulation of the RHS vortex core, substitute Eq. (11) into Eq. (15) and apply the formula

$$\Gamma_a = \int_0^\infty \int_0^\infty \omega_x \, dz \, dy \tag{16}$$

where Γ_a is the actual circulation of the RHS model vortex, as opposed to its input value Γ_i. The circulation ratio Γ_a/Γ_i is found to be[17]

$$\frac{\Gamma_a}{\Gamma_i} = \mathrm{erf}\left(z_i \sqrt{\frac{\pi \omega_i^{\max}}{\Gamma_i}} \right) \mathrm{erf}\left(y_i \sqrt{\frac{\pi \omega_i^{\max}}{\Gamma_i}} \right) \tag{17}$$

where erf is the error function:

$$\mathrm{erf}\,(b\sqrt{a}) = 2\sqrt{\frac{a}{\pi}} \int_0^b e^{-ap^2} \, dx \tag{18}$$

Thus we find that the vortices in Figs. 10 and 12 are about 1–2% weaker than their counterparts in Figs. 5 and 7. The vortices in Fig. 11 are about 10% weaker than their counterparts in Fig. 6.

Summary

The low-profile wishbone generator sheds a strong pair of counter-rotating vortices. Measurements of velocity in a downstream cross plane form the basis for characterization of the vortex structures. Vortex structure was quantified by three descriptors. Vortex strength was characterized by its circulation or integrated streamwise vorticity, vortex concentration by the magnitude of peak vorticity, and the vortex trajectory by the location of peak vorticity.

Measurements made at two axial locations illustrate the streamwise development of the shed vortices. The counter-rotating pair of vortices was observed to lift off the surface quickly. A single region of streamwise velocity deficit was located between vortex cores. Although the observed three-dimensional flow structure was complex, the flow in the cross plane is well represented by the two-dimensional Oseen model, particularly in the case of the larger vortex generator.

Acknowledgments

The authors are indebted to the project support provided by David Sheldon and Victor Canacci, operation engineers for NASA's Aeropropulsion Facilities and Experiments Division, and the rest of the very capable staff of the Icing Research Tunnel. Also, a special thank you to Bruce Reichert, of NASA's Internal Fluid Mechanics Division, for his insightful analysis of the data.

References

[1]Lin, J. C., Howard, F. G., and Selby, G. V., "Turbulent Flow Separation Control Through Passive Techniques," AIAA Paper 89-0976, March 1990.

[2]McCormick, D. C., "Shock-Boundary Layer Interaction Control with Low Profile Vortex Generators and Passive Cavity," AIAA Paper 92-0064, Jan. 1992.

[3]Reichert, B. A., and Wendt, B. J., "An Experimental Investigation of S-Duct Flow Control Using Arrays of Low Profile Vortex Generators," AIAA Paper 93-0019, Jan. 1993.

[4]Lin, J. C., Selby, G. V., and Howard, F. G., "Exploratory Study of Vortex-Generating Devices for Turbulent Flow Separation Control," AIAA Paper 91-0042, Jan. 1991.

[5]Westphal, R. V., Pauley, W. R., and Eaton, J. K., "Interaction Between a Vortex and a Turbulent Boundary Layer—Part 1: Mean Flow Evolution and Turbulence Properties," NASA TM 88361, Jan. 1987.

[6]Wendt, B. J., Greber, I., and Hingst, W. R., "The Structure and Development of Streamwise Vortex Arrays Embedded in a Turbulent Boundary Layer," *AIAA Journal*, Vol. 31, No. 2, 1993, pp. 319–325.

[7]Wheeler, G. O., "Means for Maintaining Attached Flow of a Flowing Medium," United States Patent 4,455,045, June 1984.

[8]Reichert, B. A., and Wendt, B. J., "A New Algorithm for Five-Hole Probe Calibration, Data Reduction, and Uncertainty Analysis," NASA TM 106458, March 1994.

[9]Moffat, R. J., "Contributions to the Theory of Single-Sample Uncertainty Analysis," *Transactions of the American Society of Mechanical Engineers*, Vol. 104, No. 2, 1982, pp. 250–258.

[10]Wendt, B. J., Greber, I., and Hingst, W. R., "The Structure and Development of Streamwise Vortex Arrays Embedded in a Turbulent Boundary Layer," AIAA Paper 92-0551, Jan. 1992.

[11]Anderson, B. H., and Gibb, J., "Application of Computational Fluid Dynamics to the Study of Vortex Flow Control for the Management of Inlet Distortion," AIAA Paper 92-3177, July 1992.

[12]Cho, S. Y., and Greber, I., "Three Dimensional Compressible Turbulent Flow Computations for a Diffusing S-Duct With/Without Vortex Generators," Ph.D. Dissertation, Department of Mechanical and Aerospace Engineering, Case Western Reserve Univ., Cleveland, OH, Nov. 1992.

[13]Taylor, H. D., and Grose, R. M., "Theoretical and Experimental Investigation of Various Types of Vortex Generators," United Aircraft Corporation, Research Dept. Rept. R-15362-5, East Hartford, CT, March 1954.

[14]Pearcy, H. H., "Shock-Induced Separation and Its Prevention by Design and Boundary Layer Control," *Boundary Layer and Flow Control*, Vol. 2, edited by G. V. Lachmann, Pergamon, New York, 1961, pp. 1166–1344.

[15]Eibeck, P. A., and Eaton, J. K., "An Experimental Investigation of the Heat-Transfer Effects of a Longitudinal Vortex Embedded in a Turbulent Boundary Layer," Stanford Univ., TR MD-48, Stanford, CA, Nov. 1985.

[16]Pauley, W. R., and Eaton, J. K., "The Fluid Dynamics and Heat Transfer Effects of Streamwise Vortices Embedded in a Turbulent Boundary Layer," Stanford Univ., TR MD-51, Stanford, CA, Aug. 1988.

[17]Wendt, B. J., Greber, I., and Hingst, W. R., "The Structure and Development of Streamwise Vortex Arrays Embedded in a Turbulent Boundary Layer," NASA TM 105211, Sept. 1991.

[18]Squire, H. H., "The Growth of a Vortex in Turbulent Flow," *Aeronautical Quarterly*, Vol. 16, Aug. 1965, pp. 302–306.